Author's post print PDF

Nitrogen-doped carbon foams synthesized from banana peel and zinc complex template for adsorption of CO_2, CH_4 and N_2

Arash Arami-Niya, Thomas E. Rufford and Zhonghua Zhu*

School of Chemical Engineering, The University of Queensland, St Lucia 4072 Australia

*Corresponding author: t.rufford@uq.edu.au

Keywords Carbon foam, biomass wastes, nitrogen doping, gas separation, CO_2 capture.

Abstract

We report nitrogen-doped, activated carbon foams prepared from banana peels using a self-template method with zinc nitrate, 2-aminophenol-and furfural involved. Importantly, we have extended the banana peel zinc complex soft-template method to investigate the effects of carbonization temperature and post-carbonization CO_2 activation on the carbon pore structure, and examined the effect of N-content on the carbon foam's equilibrium adsorption capacity for

CO_2. The carbon foams contain up to 6.0 %wt nitrogen, and feature cellular macroporous structures with BET specific surface areas up to 1426 $m^2.g^{-1}$. The potential of the carbon foams for CO_2/N_2, CO_2/CH_4 and CH_4/N_2 separations was evaluated by measurement of pure fluid adsorption capacities using a gravimetric adsorption apparatus and calculation of adsorption selectivies at a range of conditions using Ideal Adsorption Solution Theory (IAST). The adsorption capacities at a 4000 kPa and 298 K were CO_2 9.21 $mmol.g^{-1}$, CH_4 5.29 $mmol.g^{-1}$ and N_2 3.29 $mmol.g^{-1}$.

1 Introduction

Carbon foams with high void volumes, hierarchical porous structures, low bulk density, and good thermal and electrical conductivity have been reported as catalyst supports, energy storage electrodes, insulation materials and adsorbents [1, 2]. Carbon foams can be prepared from coal tar pitch and petroleum pitch [3, 4], polymeric precursors [5] or renewable biomass-based precursors such as sucrose [6] and banana peel [7]. Renewable biomass materials for carbon foams may offer long-term environmental and economic advantages to fossil-fuel sources such as pitch. In addition, biomass materials can provide interesting natural macroporous structures and chemical compositions that may be utilised to create novel foam properties.

Banana peel (BP) is an agricultural waste available in large volumes as bananas are a very popular and nutritionally important fruit for a wide population of the world - the global production of bananas is more than 100 million tonnes annually[8]. Our collective appetite for bananas generates a large volume of waste banana peels as the peel typically represents 30 - 40 % of the banana's weight[9, 10] and, although most bananas are consumed raw or cooked in

domestic contexts there are still large volumes of waste BP produced in industrial food processing plants and these peels are typically disposed to landfill. Alternatives to disposal of waste banana peels from food processing plants to landfills include utilisation of the waste BP in biogas generation [11], extraction of aromatic compounds[10] and production of activated carbon adsorbents[12, 13].

Banana peels contain a diverse mix of biopolymers including pectin, hemicellulose, cellulose, and lignin [9, 14]. Of particular relevance to our current work on carbon foams are the gel-forming properties of BP-pectins [9] and the polar surface functional groups on various BP compounds, which can act as sites for metal ion complexation (often cited for use in heavy metal ion adsorption[15, 16]). Lv et al.[7] utilised both BP's gel-forming properties and metal-complexation sites to adsorb phenolic resin-precursors to produce self-templated hierarchical carbon foams for supercapacitor electrodes. In this procedure, the introduction of 2-aminophenol to the carbon provides nitrogen-containing functional groups on the carbon foam that may present attractive properties for supercapacitor electrodes (as evaluated by Lv et al.[7]) and enhanced CO_2 adsorption. In this study, we extend the self-templated carbon foam synthesis methods proposed by Lv et al.[7], and others [17, 18] to investigate the effects of carbonization temperature and post carbonization CO_2 activation on the carbon foam structure. We also examine the influence of the carbon foam's nitrogen content on the adsorption equilibrium capacities of CO_2, CH_4 and N_2.

2 Experimental methods

2.1 Materials

Queensland-grown yellow Cavendish bananas (*Musa acuminate*) were purchased from a local supermarket in Brisbane. After the first author ate the fruit, the banana peels were washed in

distilled water, dried in air overnight and sliced into small pieces. Reagent grade zinc nitrate hexahydrate ($Zn(NO_3)_2.6H_2O$), furfural ($C_5H_4O_2$) and 2-aminophenol (C_6H_7NO) were used without further purification. The purities of gases used in this work, as stated by the supplier Coregas Australia, were 99.999 % for helium, argon and nitrogen; and 99.995 % for carbon dioxide and methane.

2.2 Preparation of nitrogen-doped carbon foams

The procedure to prepare carbon foams was based on the self-template method proposed by Lv et al. [7] using zinc ions coordinated with carboxylic and hydroxyl groups on the BP's pore surfaces. The key process steps in this procedure, as summarised in Figure 1, were: (1) The BP particles were soaked in 2 $mol.L^{-1}$ zinc nitrate solution at 343 K in a closed vessel for 7 days to form zinc complexes. (2) The reaction vessel was opened and the excess water was evaporated over 14 days at 333 K to obtain brown zinc complexes. (3) The zinc complexes were soaked in a mixture of furfural and 2-aminophenol at 343 K for 7 days. This step produces a slurry of banana peel zinc complexes impregnated with a 2-aminophenol-furfural resin, which subsequently provides a N-rich carbon source during pyrolysis. We refer to the resin filled intermediate product obtained in this step as the banana peel composite or BPC. (4) 7 g of the slurry was pressed by hand into a cylindrical quartz crucible (2.54 cm diameter × 2.54 cm height), dried at 393 K overnight and carbonized in a horizontal tube furnace at temperatures in the range of 1023 – 1273 K for carbonization times of 1 to 11 hrs. In addition, we extended Lv et al.'s procedures [7] to produce a set of CO_2 activated carbon foams by switching the gas flow from argon to CO_2 once the carbonization temperature had been reached. The heating rate in all experiments was 10 $K.min^{-1}$. Carbons produced from the banana peel zinc complexes are

labelled as chemically-modified banana foams CBF-T-FF-t, where T = [1023 - 1273] K, FF is the gas atmosphere and t the duration of the carbonization step.

We also prepared carbons by direct pyrolysis of the sliced BP in argon at 873 K to produce BP-char (heating rate = 10 K min^{-1}; hold time = 1 hr) and by CO_2 activation of this char to produce activated BP carbons (BPAC). The CO_2 activation was performed after the char had cooled in argon, and then the gas was switched to 50 mL.min^{-1} CO_2 and the furnace temperature increased again at 10 K.min^{-1} to 1023 K for 1 or 3 hours. These samples were labelled BPAC followed by the activation temperature, gas type and activation duration.

The yield of each carbon product in the pyrolysis or pyrolysis plus carbonization steps was calculated as:

$$Yield(\%) = (\frac{W_f}{W_i}) \times 100 \qquad (1)$$

where W_i and W_f are the dry weight (g) of feed for each process (BP, BP char or impregnated BP) and dry weight (g) of products (bio-char, BPACs or CBFs), respectively. The uncertainty in the weight measurements was less than 1.4 % and the carbon yields obtained across at least three repeat experiments varied by less than 2 %wt.

2.3 Characterizations

The carbons were characterized by scanning electron microscopy (SEM, JEOL JSM-6100), energy-dispersive x-ray spectroscopy (EDX, also with JEOL JSM-6100), thermogravimetric analysis (TGA, Perkin Elmer STA 6000) and X-ray photoelectron spectroscopy (XPS, Kratos Axis ULTRA X-ray photoelectron spectrometer using a monochromated Al Kα (1486.6 eV) excitation source). The quantitative analysis of XPS data was performed with CasaXPS software

after Shirley background subtraction. Bulk concentrations of C, H and N were determined with an Elemental Analyzer (FlashEA1112 series), and the O concentrations were assumed to be the residual between 100 % and the sum of C, H and N concentrations. For each sample three CHNS measurements were made and we report the mean of the three measurements (a typical standard deviation was 0.7%wt.).

Pore textural properties of the carbon foams were characterised by mercury intrusion porosimetry (MIP) measured at pressures in the range 20 – 414000 kPa (Micromeritics PoreSizer 9320), and sorption analyses with CO_2 at 273 K and N_2 at 77 K (Micromeritics TriStar II 3020). Samples were degassed at 473 K and a pressure of 10^{-5} torr for 24 hr prior to CO_2 and N_2 sorption measurements. Specific surface areas (S_{BET}) were calculated by the Brunauer-Emmett-Teller method at the relative pressures in the range of P/P_0 = 0.05 - 0.30; total pore volumes were estimated at P/P_0 = 0.98; and volumes of micropores were calculated from both the 77 K N_2 and 273 K CO_2 isotherms using the Dubinin-Astakhov (D-A) equation. [19, 20] The micropore surface area was calculated using Dubinin-Radushkevich (D-R) equation with the CO_2 isotherm measured at 273 K. The pore size distributions (PSD) were determined using a density functional theory model (DFT) algorithm for carbon slit pores supplied with the Micromeritics instrument.

2.4 Gravimetric adsorption equilibria measurement

Adsorption isotherms of pure fluids CO_2, CH_4, and N_2 were measured at (298, 313 and 323) K and pressures up to 4000 kPa using a BELSORP-BG instrument (BEL Japan) equipped with a RUBOTHERM magnetic floating balance. Prior to adsorption measurements the carbon foam was degassed in-situ at 473 K for 24 hrs. We have described elsewhere the operation of this

apparatus to measure adsorption on carbon materials [19], so we only include here in the Supporting Information a brief description of the BELSORP-BG measurement procedures.

3 Results and discussions

3.1 Preparation of chemically modified banana peel foam monoliths

The SEM images in Figure 2 show the natural structure raw banana peel features open cell structures that are approximately 5 – 20 μm wide and the cell walls are coated in biopolymers. The total nitrogen concentration of the raw BP determined by the CHNS Elemental Analyser was 1.9 %wt (Table 1), which is comparable to the nitrogen concentrations in banana peels reported in other studies[14]. Proximate analysis of the raw BP by thermal gravimetric analysis obtained 67.7 %wt volatiles, 24.2 %wt fixed carbon and 8.2 %wt ash. The dried (samples were dried at 473 K under nitrogen) raw BP's residual mass after the TGA measurement shown in Figure 3 is consistent with the yield of 38.8 %wt BP-char produced by pyrolysis of raw BP in the tube furnace (Table 1).

The TGA weight loss curve in Figure 3 of the banana peel treated with zinc nitrate and impregnated with the furfural + 2-aminophenol resin (dry basis) shows that the BPC composite has a greater thermal stability than the raw BP at temperatures in the range 500 - 773 K; this BPC weight loss curve is consistent with the decomposition of aminophenol-furfural resins reported in the literature. For example, Patel et al.[20] report aminophenol-furfural resins will soften at temperatures above 473 K and then harden at temperatures from 703 - 843 K due to de-volatilization of the resin and BP polymers. The BPC weight loss observed in Figure 3 at temperature above 1100 K includes the evaporation of zinc via reduction of ZnO (derived from the zinc nitrate) to metallic zinc [21, 22], and the EDX spectra for BPC, CBF-1023-Ar-3h and CBF-

1273-Ar-3h confirms the loss of zinc from the composite after pyrolysis at 1273 K (see Fig. S2). Table 1 shows the yields of CBFs produced in argon ranged from 65.7 %wt to 23.6 %wt; the yield decreased at higher temperatures and longer carbonization time.

An aim of this study was to produce monolithic carbon foams with a mechanically stable, open cellular structure and the chemically-modified banana foam synthesis method successfully produced monoliths of CBF, as summarised in Table 1. All the CBF products were stable solid discs that retained the cylindrical shape of the crucible and the inset photograph for CBFs in Figure 1 shows a typical example of a CBF disc. In contrast, BPAC-1023-CO_2-1h produced by th more conventional carbonization and CO_2 activation process was a loose agglomeration of granules that was easily crumbled by hand.

The SEM images of CBF-1273-Ar-3h in Figure 4a-c show a highly porous foam-like open cell structure with typical carbon foam features of ligaments and walls [23, 24]. Clearly, the texture of the CBF sample is different to the texture of the BPAC-1023-CO_2-1h produced by CO_2 activation of BP (Figure 4g-i). Mercury intrusion porosimetry (Figure 5) shows a broad distribution of macroporous channels in CBF-1273-Ar-3h, the largest channels are approximately 80 μm wide. These results demonstrate that direct CO_2 activation of BP does not produce the carbon foam structure, so we may infer that the porous structure developed in the CBFs results partly from the devolitisation and polymerisation of furfural-aminophenol resin.

The furfural-aminophenol resin carbonization may be considered a bubble growth foaming process, which in our study is template by the BP structure. Beecham et al. [25] described three key stages in a bubble growth foaming process: firstly, the resin melts around 473 K; secondly as the temperature increases light hydrocarbons such as unreacted furfural evolve from the resin; and

thirdly the polymerisation of the resin leads to evolution of gaseous reaction products and an increase in the viscosity of the resin. After these three stages and at temperatures between 703 - 843 K the molten resin has reacted to such a degree that the resin solidifies. The TGA curves shown in Figure 3 support this mechanism. Additionally, in the presence of the BP-zinc nitrate complex the biopolymers of the BP which are mostly released from raw BP at temperatures below 673 K (Figure 3) may provide additional gas for bubble formation and growth in the resin phase.

Table 1 summarises the elemental concentrations of nitrogen in the carbons. The bulk nitrogen concentration of CBF-1023-Ar-3h was 6.0 %wt, which is 2.6 times the nitrogen content of the activated carbon BPAC-1023-CO_2-1h, and the primary source of additional nitrogen in the chemically-modified CBFs is the 2-aminophenol (C_6H_7NO contains 12.83 %wt N). The intermediate BPC contained 8.0 %wt N and XPS characterisation, as shown in Figure 6a and Table 3, confirms the BPC surface features amine groups (N-1 at binding energy (BE) of 399.4 ± 0.1 eV)[26-28] and amides (N-2 at BE = 400.5 ± 0.1 eV) from the 2-aminophenol-furfural resin[20]. The N-3 group detected around BE = 407.3 ± 0.1 eV in the XPS of BPC may be attributed to unreacted nitrate salts from the zinc nitrate reagent. [26-29]

Carbonization at higher temperature (1273 K) and longer duration (8 h and 11 h) decomposed some N-functional groups on the carbon surface to reduce total N concentrations in the CBFs to 4.6 - 3.9 %wt. The XPS data for CBF-1273-Ar-3h in Figure 6b and Table 3 also show that after carbonization at 1273 K the nitrogen from 2-aminophenol is converted to pyridinic-N (N-4, BE = 398.2 ± 0.1 eV), pyrrolic/pyridone-N (N-5, BE = 399.8 ± 0.1 eV), and quaternary-N (N-6, BE= 401.1 ± 0.1 eV) sdattructures.[30, 31] These results are consistent with other reports on the

carbonization of N-rich precursors to introduce nitrogen to carbon frameworks.[32-34] For example, at temperature above 873 K pyridinic and pyrrolic structures are produced by decomposition of amide groups [35] and the reaction of NO_3 with carbon; and Chambrion et al.[30] proposed C-NO reactions that lead to quaternary-N.

3.2 Development of microporosity in the carbon foams

N_2 sorption isotherms were measured at 77 K on the BPAC-1023-CO_2-1h and CBFs and are shown in Figure 7a. A summary of pore structure properties is provided in Table 2. The BP-char was not expected to have a well-developed pore structure at the char preparation conditions[36] and so we were not able to measure a useful N_2 sorption isotherm at 77 K on BP-char. The N_2 isotherm of the CO_2 activated carbon BPAC-1023-CO_2-1h presents a composite of Types I and II isotherms according to the 2015 IUPAC classifications, [37] with a type H4 hysteresis loop at relative pressures around $P/P_0 = 0.8$ which is representative of sorption behaviour in a carbon featuring both micropores and mesopores. The pores size distribution in Figure 7b shows BPAC-1023-CO_2-1h has a bimodal distribution of micropores around 13 Å and small mesopores around 20 – 25 Å.

The N_2 isotherms of the CBFs prepared under argon also feature hysteresis loops that suggest the presence of mesopores together with a degree of microporosity. As indicated by the uptake of N_2 at 77 K (Figure 7a) and the calculated D-R micropore N_2 accessible surface areas, the microporosity of CBFs prepared under argon treatment for 3 hr increased almost two-fold at 1273 K compared to the CBF produced at 1023 K, and prolonged carbonization times produced a further increase in micropore surface area of about 15 % (D-R micropore surface area). The trends in micropore areas and volumes determined from CO_2 isotherms measured at 273 K

(Figure 8a), and pore texture parameters in Table 2 derived from CO_2 isotherms, are consistent with the N_2 sorption results. The evaporation of ZnO particles from the carbon structure is likely to be one reason for the greater volume of micropores produced at a carbonization temperature of 1273 K.

The CBF with the highest surface area prepared under argon without CO_2 activation was CBF-1273-Ar-11h with a BET surface area of 190.4 $m^2.g^{-1}$ and CO_2 D-R micropore surface area of 628.5 $m^2.g^{-1}$. However, the yield of this CBF was significantly lower than the yield of CBF-1273-Ar-3h. The BET surface area of CBF-1273-Ar-11h is similar to that of activated carbon BPAC-1023-CO_2-1 (204.3 $m^2.g^{-1}$), but the CBFs have both larger N_2-accesible pore volumes and narrow micropore volumes as measured by CO_2 sorption (Table 2). Notably, the CBFs produced in this study have lower surface areas and pore volumes than the foams reported by Lv et al. [7]. A possible explanation for the difference in the results could be that the ratio of furfural-aminophenol resin to BP used in the resin impregnation stage of our experiments was different to the ratio used by Lv et al.. This experimental detail was not reported in the previous studies. To summarize, the results of our experiments with CBFs prepared in argon suggest (1) that the optimum carbonization temperature to maximise surface area under argon is 1273 K, and (2) carbonization at 1273 K for more than 3 h enhances micropore development but this additional porosity is obtained with a reduced product yield.The effect of the CO_2 activation step on micropore development in CBFs is highlighted by the N_2 and CO_2 sorption isotherms for CBF-1023-CO_2-3h shown in Figure 7a and Figure 8a. Even at a carbonization temperature of 1023 K, the CO_2 activated CBF has a BET area of more than 350 $m^2.g^{-1}$ and CBF-1023-CO_2-3h has twice the total pore volume of the CBF-1023-Ar-3h (Table 2, from the N_2 77 K isotherm). The CO_2 activation process acts to widen a broad range of pore sizes - as evidenced by the increase in

macropore volume measured by MIP (Figure 5) and the increase in pore volume for widths from 10 -40 Å determined from the N_2 sorption (Figure 7b). Under CO_2 activation conditions, like in the case of argon-carbonized CBFs, the surface area and micropore volumes increase with the carbonization temperature to a maximum BET area of 1426.1 $m^2.g^{-1}$ for CBF-1273-CO_2-1h. The yield of CBF-1273-CO_2-1h was 14.2 %wt so by this method there is a high yield penalty to produce the highest surface area CBF. We attempted to produce a CO_2 activated CBF at 1273 K treated in CO_2 for 3 h (i.e. CBF-1273-CO_2-3h) but this activation condition consumed almost all the carbon and there was insufficient product recovered from the furnace to be characterized.

3.3 Adsorption equilibria of pure gases

The CO_2 adsorption capacities of the CBFs and BPAC measured on the Tristar II at 273 K and 303 K and pressures up to 130 kPa are shown in Figure 8a and Figure 9. As might be expected, the carbon with the highest capacity for CO_2 at these conditions was the CBF with the highest surface area and micropore volume - that is CBF-1273-CO_2-1h (5.75 $mmol.g^{-1}$). The CBFs exhibit higher capacity for CO_2 than some other reported carbon foams with similar micropore surface areas. For example, at 273 K, Tsyntsarki et al.[38] reported 3.35 $mmol.g^{-1}$ CO_2 on a pitch-derived and steam activated foam with BET of 933 $m^2.g^{-1}$ and Liu et al.[17] reported 2.35 $mmol.g^{-1}$ CO_2 on nitrogen-doped porous carbons with a surface area of a 1148 $m^2.g^{-1}$. This second example was prepared from banana peels using an aluminium nitrate synthesis procedure similar to the zinc nitrate method we used. Table 5 presents additional examples of CO_2, CH_4 and N_2 adsorption capacities at conditions close to ambient temperatures on carbon monoliths, a commercial activated carbon, zeolite 13X and metal organic frameworks that can be used to place the adsorption capacity of CBF-1273-CO_2-1h in context with other reported materials. The

CBF adsorption capacity is similar to many other carbon materials; but we note that the CO_2 uptakes are not as high as some metal organic frameworks (MOFs) reported in the literature[39].

The effect of the CBFs' nitrogen functional groups on CO_2 adsorption capacities were normalised for micropore surface area as shown in Figure 10a and on this basis CBP-1023-Ar-3h has the highest CO_2 adsorption capacity per m^2 of micropore surface area. The value of CO_2 uptake divided by micropore surface area of the CBFs (Figure 10a) is higher than almost all the biomass based activated carbons and nitrogen-modified activated carbons reported on the recent review by Rashidi and Yusup [40]. Figure 10b shows an alternate analysis in which we normalised CO_2 adsorption capacities for bulk nitrogen concentrations and plotted this capacity against the micropore surface area. CO_2 adsorption analysis of the CBFs at 303 K (Figure 9) showed BPAC-1023-CO_2-1h with the lowest micropore surface area and nitrogen contents obtained the lowest and CBF-1273-CO_2-1h with the highest measured micropore surface area and 4.2% nitrogen content the highest CO_2 capture. These low pressure CO_2 adsorption results are consistent with other studies that conclude both nitrogen functional groups and microporosity are important parameters in CO_2 adsorption performance of activated carbons [41, 42].

Based on the CO_2 equilibrium capacities measured at low pressure we selected CBF-1273-CO_2-1h for further measurements in the high-pressure gravimetric adsorption apparatus at temperatures of (298,313 and 323) K. The absolute adsorption capacities of CO_2, CH_4 and N_2 on CBF-1273-CO_2-1h are shown in Figure 11 to Figure 13. The high-pressure adsorption equilibria data is also included in Table S 1 of the Supporting Information. We also measured at 298 K the absolute adsorption capacities CO_2, CH_4 and N_2 on CBF-1273-Ar-3h (Figure 14 and Table S 2). Compared to the CO_2, CH_4 and N_2 adsorption capacities of other carbon adsorbents reported in

the literature, CBF-1273-Ar-3h has a reasonable capacity for these gases [43-45]. As expected, the adsorption capacities on the carbon foam prepared under argon were lower than the capacities on CO_2 activated CBF-1273-CO_2-1h. The adsorption capacities for CO_2, CH_4 and N_2 on CBF-1273-CO_2-1h measured at 298 K and 4000 KPa were about 63 %, 76 % and 34% higher, respectively, than the capacities on CBF-1273-Ar-3h. This comparative results highlights that the CO_2 activation of the foam has improved the selectivity of the CBF for CO_2 and CH_4 over N_2.

The adsorption uptake of CO_2 on CBF-1273-CO_2-1h at 298 K and 4000 kPa is 9.21 mmol.g^{-1}, which is higher than most of the activated carbon monoliths and other carbon foams reported [24]. For example, Narasimman et al. [46] reported a CO_2 capacity of 2.5 mmol g^{-1} at 298 K and 2000 kPa on carbon foams prepared from molten sucrose using an aluminium nitrate blowing agent; Dassanayake et al.[47] reported a CO_2 capacity of 3.7 mmol g^{-1} at 298 K and 1200 kPa on cellulose-based aerogel; and Ribeiro et al.[48] measured CO_2, CH_4 and N_2 adsorption capacity of 4.7, 2.9 and 1.5 mmol.g^{-1}, respectively, on activated carbon honeycomb monolith at 299 and pressure of about 600 kPa. The CO_2 uptake on CBF-1273-CO_2-1h is also higher than the capacity of activated carbon monolith derived from tar pitch and coal produced in our laboratory recently (7.4 mmol CO_2 g^{-1} at 298 K and 3500 kPa) [19].

A temperature-dependent, semi-empirical Toth isotherm model was tested to determine the ability of CBF-1273-CO_2-1h to predict adsorption capacities of CO_2, CH_4 and N_2 across the range of pressure and temperature conditions measured in this study. We used the fitted Toth isotherm models and an Ideal Adsorption Solution Theory (IAST) model to predict selectivity for separating CO_2 + CH_4, CO_2 + N_2 and CH_4 + N_2 gas mixtures. The Toth isotherm model is described by Equation 2 [49]:

$$Q_{\mu i}^{Toth} = Q_{\mu si}^{Toth} \frac{b_i P}{\left[1+(b_i P)^{t_i}\right]^{1/t_i}} \quad \text{with} \quad b_i = b_{o,i} \exp\left(\frac{-\Delta H_{Toth,i}}{RT}\right) \tag{2}$$

where R is the molar gas constant, P and T are the measurement pressure and temperature. In the regression of this model, $\Delta H_{Toth,i}$ was treated as an adjustable parameter together with the empirical parameters ($Q_{\mu si}^{calc}$, $b_{0,i}$ or t_i). The parameters t_i is used to characterise the heterogeneity of the adsorption sites in the model, but it was treated as adjustable parameter in the regression. The best fit parameters of Equation 2 were determined using a least-squares regression analysis to minimize the standard deviation (SD) between the measured capacities, Q_{μ}, and the capacities $Q_{\mu si}^{calc}$ calculated with the model ($SD = ((1/N)\Sigma(Q_{\mu i}^{meas} - Q_{\mu i}^{calc})^2)^{1/2}$ where N is the number of data points regressed).

Table 4 lists the optimized parameters of Equation 2 and the standard deviations (SD) resulting from the regression of the Toth model to the CBF-1273-CO_2-1h high pressure adsorption data. Deviations $(Q_{\mu}^{meas} - Q_{\mu}^{calc})$ between the measured and the calculated capacities of Toth model that are shown in Figure 11b, Figure 12b and Figure 13b are in the range of ± 0.1 at most of the pressure points. This isotherm model has a SD of 0.083 mmol.g^{-1} for CO_2, 0.035 mmol.g^{-1} for CH_4 and 0.009 mmol.g^{-1} for N_2.

The adsorption equilibrium selectivity for separating CO_2 + CH_4, CO_2 + N_2 and CH_4 + N_2 gas mixture pairs on the CBF-1273-CO_2-1h were evaluated using the IAST[50] implemented for the Toth isotherm parameters using the algorithm of Valenzuela and Myers[51] without adjustment of the pure fluid isotherm parameters. Figure 15 shows the predicted selectivity in equimolar binary gas mixtures at pressures up to 3000 kPa. The selectivities predicted with IAST at 298 K and

100 kPa for the three gas mixtures at different compositions are included in Fig S3(a-c) of the Supporting Information. In equimolar gas mixtures at 298 K, the predicted selectivity of CBF-1273-CO_2-1h is up to 16 at low pressures for CO_2 from N_2 and approximately four for both CO_2 from CH_4 and CH_4 from N_2. The CO_2 selectivity of this CBF is about 1.5 times higher than the selectivity of our previously reported coal + pitch based activated carbon monolith[19] and higher than some other reported structured carbons[6, 46, 48], biomass based activated carbons[40] and commercial activated carbons[41, 45]. Clearly, the CO_2 selectivity of CBF-1273-CO_2-1h is not as great as metal organic frameworks (MOFs)[52] and modified carbons[17]. Nonetheless, these results show that the nitrogen-doped banana-peel carbon foam CBF-1273-CO_2-1h has some potential for CO_2 capture and other adsorption applications.

4 Conclusions

Monolithic carbon foams with an open cellular structure were successfully produced from banana peel using a soft-template method with zinc nitrate, furfural and 2-aminophenol. CO_2 activation of the chemically-modified banana peel foams developed large micropore voluems and high surface areas in the carbon foams. After carbonization of the precursors at 1273 K the nitrogen from 2-aminophenol and any naturally occurring N in the banana peel was converted to pyridinic-N, pyrrolic/pyridone-N, and quaternary-N structures, and the presence of this N in the carbon foams was found to enhance CO_2 adsorption capacity on the carbons. The carbon foam CBF-1273-CO_2-1h exhibited the highest CO_2 and CH_4 adsorption capacities and the most promising CO_2/N_2 equilibrium selectivity in this study. Future challenges to develop this class of carbon foam materials may be to find alternative complexing agents that have a lower

environmental toxicity to the zinc salts used in this study and to investigate the production of CO_2 activated carbons directly from the furfural + aminophenol resin.

Acknowledgements

This research was funded by the Australian Research Council (DE140100569, FT120100720) with additional scholarship support for Mr Arami-Niya provided through a UQ International Postgraduate Research Scholarship. We thank Dr Ge Lei for technical assistance in the laboratory, Miss Yangyang Wen for assistance with the CHNS measurements and Dr Barry Wood for assistance with XPS. We acknowledge the facilities and technical assistance of the Australian Microscopy & Microanalysis Research facility at the Centre for Microscopy & Microanalysis at the University of Queensland.

Supporting Information. A description of the gravimetric adsorption apparatus, SEM, EDX spectra, tabulated high pressure adsorption data, IAST equilibrium selectivity calculations.

References

1. Inagaki, M.; Kang, F.; Toyoda, M.; Konno, H., Chapter 9 - Carbon Foams. In *Advanced Materials Science and Engineering of Carbon*, Inagaki, M.; Kang, F.; Toyoda, M.; Konno, H., Eds. Butterworth-Heinemann: Boston, 2014; pp 189-214.
2. Asfaw, H. D.; Roberts, M.; Younesi, R.; Edstrom, K., Emulsion-templated bicontinuous carbon network electrodes for use in 3D microstructured batteries. *Journal of Materials Chemistry A* **2013,** 1, (44), 13750-13758.
3. Chen, C.; Kennel, E. B.; Stiller, A. H.; Stansberry, P. G.; Zondlo, J. W., Carbon foam derived from various precursors. *Carbon* **2006,** 44, (8), 1535-1543.
4. Hao, G.-P.; Li, W.-C.; Qian, D.; Wang, G.-H.; Zhang, W.-P.; Zhang, T.; Wang, A.-Q.; Schüth, F.; Bongard, H.-J.; Lu, A.-H., Structurally Designed Synthesis of Mechanically Stable Poly(benzoxazine-co-resol)-Based Porous Carbon Monoliths and Their Application as High-Performance CO2 Capture Sorbents. *Journal of the American Chemical Society* **2011,** 133, (29), 11378-11388.
5. Inagaki, M.; Morishita, T.; Kuno, A.; Kito, T.; Hirano, M.; Suwa, T.; Kusakawa, K., Carbon foams prepared from polyimide using urethane foam template. *Carbon* **2004,** 42, (3), 497-502.
6. Narasimman, R.; Prabhakaran, K., Preparation of low density carbon foams by foaming molten sucrose using an aluminium nitrate blowing agent. *Carbon* **2012,** 50, (5), 1999-2009.
7. Lv, Y.; Gan, L.; Liu, M.; Xiong, W.; Xu, Z.; Zhu, D.; Wright, D. S., A self-template synthesis of hierarchical porous carbon foams based on banana peel for supercapacitor electrodes. *Journal of Power Sources* **2012,** 209, (0), 152-157.
8. Food and Agriculture Organization of the United Nations FOASTAT. http://faostat3.fao.org/home/E
9. Emaga, T. H.; Robert, C.; Ronkart, S. N.; Wathelet, B.; Paquot, M., Dietary fibre components and pectin chemical features of peels during ripening in banana and plantain varieties. *Bioresource Technology* **2008,** 99, (10), 4346-4354.
10. Ji, L.; Srzednicki, G., Extraction of aromatic compounds from banana peels. In *Acta Horticulturae*, 2015; Vol. 1088, pp 541-546.
11. Clarke, W. P.; Radnidge, P.; Lai, T. E.; Jensen, P. D.; Hardin, M. T., Digestion of waste bananas to generate energy in Australia. *Waste Management* **2008,** 28, (3), 527-533.
12. Gupta, H.; Gupta, B., Adsorption of polycyclic aromatic hydrocarbons on banana peel activated carbon. *Desalination and Water Treatment* **2016,** 57, (20), 9498-9509.
13. Ma, J.; Huang, D.; Zou, J.; Li, L.; Kong, Y.; Komarneni, S., Adsorption of methylene blue and Orange II pollutants on activated carbon prepared from banana peel. *Journal of Porous Materials* **2015,** 22, (2), 301-311.
14. Jiang, R.; Sun, S.; Xu, Y.; Qiu, X.; Yang, J.; Li, X., Leaching behavior of total organic carbon, nitrogen, and phosphorus from banana peel. *Water Science and Technology* **2015,** 71, (10), 1458-1462.
15. Memon, J. R.; Memon, S. Q.; Bhanger, M. I.; El-Turki, A.; Hallam, K. R.; Allen, G. C., Banana peel: A green and economical sorbent for the selective removal of Cr(VI) from industrial wastewater. *Colloids and Surfaces B: Biointerfaces* **2009,** 70, (2), 232-237.
16. Thirumavalavan, M.; Lai, Y.-L.; Lin, L.-C.; Lee, J.-F., Cellulose-Based Native and Surface Modified Fruit Peels for the Adsorption of Heavy Metal Ions from Aqueous Solution:

Langmuir Adsorption Isotherms. *Journal of Chemical & Engineering Data* **2009,** 55, (3), 1186-1192.
17. Liu, R.-L.; Ji, W.-J.; He, T.; Zhang, Z.-Q.; Zhang, J.; Dang, F.-Q., Fabrication of nitrogen-doped hierarchically porous carbons through a hybrid dual-template route for CO2 capture and haemoperfusion. *Carbon* **2014,** 76, 84-95.
18. Lotfabad, E. M.; Ding, J.; Cui, K.; Kohandehghan, A.; Kalisvaart, W. P.; Hazelton, M.; Mitlin, D., High-Density Sodium and Lithium Ion Battery Anodes from Banana Peels. *ACS Nano* **2014,** 8, (7), 7115-7129.
19. Arami-Niya, A.; Rufford, T. E.; Zhu, Z., Activated carbon monoliths with hierarchical pore structure from tar pitch and coal powder for the adsorption of CO_2, CH_4 and N_2. *Carbon* **2016,** 103, 115-124.
20. Patel, P. S.; Patel, S. R., Synthesis, characterization of m-aminophenol-furfural and m-diethylaminophenol-furfural resins. *European Polymer Journal* **1987,** 23, (9), 733-735.
21. Liu, B.; Shioyama, H.; Akita, T.; Xu, Q., Metal-Organic Framework as a Template for Porous Carbon Synthesis. *Journal of the American Chemical Society* **2008,** 130, (16), 5390-5391.
22. Liu, B.; Shioyama, H.; Jiang, H.; Zhang, X.; Xu, Q., Metal–organic framework (MOF) as a template for syntheses of nanoporous carbons as electrode materials for supercapacitor. *Carbon* **2010,** 48, (2), 456-463.
23. Kumar, R.; Dhakate, S. R.; Gupta, T.; Saini, P.; Singh, B. P.; Mathur, R. B., Effective improvement of the properties of light weight carbon foam by decoration with multi-wall carbon nanotubes. *Journal of Materials Chemistry A* **2013,** 1, (18), 5727-5735.
24. Inagaki, M.; Qiu, J.; Guo, Q., Carbon foam: Preparation and application. *Carbon* **2015,** 87, 128-152.
25. Beechem, T.; Lafdi, K.; Elgafy, A., Bubble growth mechanism in carbon foams. *Carbon* **2005,** 43, (5), 1055-1064.
26. Graf, N.; Yegen, E.; Gross, T.; Lippitz, A.; Weigel, W.; Krakert, S.; Terfort, A.; Unger, W. E. S., XPS and NEXAFS studies of aliphatic and aromatic amine species on functionalized surfaces. *Surface Science* **2009,** 603, (18), 2849-2860.
27. Jansen, R. J. J.; van Bekkum, H., XPS of nitrogen-containing functional groups on activated carbon. *Carbon* **1995,** 33, (8), 1021-1027.
28. Pels, J. R.; Kapteijn, F.; Moulijn, J. A.; Zhu, Q.; Thomas, K. M., Evolution of nitrogen functionalities in carbonaceous materials during pyrolysis. *Carbon* **1995,** 33, (11), 1641-1653.
29. Krepelova, A.; Newberg, J.; Huthwelker, T.; Bluhm, H.; Ammann, M., The nature of nitrate at the ice surface studied by XPS and NEXAFS. *Physical Chemistry Chemical Physics* **2010,** 12, (31), 8870-8880.
30. Chambrion, P.; Suzuki, T.; Zhang, Z.-G.; Kyotani, T.; Tomita, A., XPS of Nitrogen-Containing Functional Groups Formed during the C−NO Reaction. *Energy & Fuels* **1997,** 11, (3), 681-685.
31. Chen, H.; Lin, G.; Chen, Y.; Chen, W.; Yang, H., Biomass Pyrolytic Polygeneration of Tobacco Waste: Product Characteristics and Nitrogen Transformation. *Energy & Fuels* **2015**.
32. Hao, G.-P.; Li, W.-C.; Qian, D.; Lu, A.-H., Rapid Synthesis of Nitrogen-Doped Porous Carbon Monolith for CO2 Capture. *Advanced Materials* **2010,** 22, (7), 853-857.
33. McGann, J. P.; Zhong, M.; Kim, E. K.; Natesakhawat, S.; Jaroniec, M.; Whitacre, J. F.; Matyjaszewski, K.; Kowalewski, T., Block Copolymer Templating as a Path to Porous

Nanostructured Carbons with Highly Accessible Nitrogens for Enhanced (Electro)chemical Performance. *Macromolecular Chemistry and Physics* **2012,** 213, (10-11), 1078-1090.
34. Hulicova-Jurcakova, D.; Kodama, M.; Shiraishi, S.; Hatori, H.; Zhu, Z. H.; Lu, G. Q., Nitrogen-Enriched Nonporous Carbon Electrodes with Extraordinary Supercapacitance. *Advanced Functional Materials* **2009,** 19, (11), 1800-1809.
35. Jansen, R. J. J.; van Bekkum, H., Amination and ammoxidation of activated carbons. *Carbon* **1994,** 32, (8), 1507-1516.
36. Marsh, H.; Rodríguez-Reinoso, F., Chapter 4 - Characterization of Activated Carbon. In *Activated Carbon*, Marsh, H.; Rodríguez-Reinoso, F., Eds. Elsevier Science Ltd: Oxford, 2006; pp 143-242.
37. Thommes, M.; Kaneko, K.; Neimark, A. V.; Olivier, J. P.; Rodriguez-Reinoso, F.; Rouquerol, J.; Sing, K. S. W., Physisorption of gases, with special reference to the evaluation of surface area and pore size distribution (IUPAC Technical Report). *Pure and Applied Chemistry* **2015,** 87, (9-10), 1051-1069.
38. Tsyntsarski, B.; Petrova, B.; Budinova, T.; Petrov, N.; Velasco, L. F.; Parra, J. B.; Ania, C. O., Porosity development during steam activation of carbon foams from chemically modified pitch. *Microporous and Mesoporous Materials* **2012,** 154, (0), 56-61.
39. Li, J.-R.; Ma, Y.; McCarthy, M. C.; Sculley, J.; Yu, J.; Jeong, H.-K.; Balbuena, P. B.; Zhou, H.-C., Carbon dioxide capture-related gas adsorption and separation in metal-organic frameworks. *Coordination Chemistry Reviews* **2011,** 255, (15–16), 1791-1823.
40. Rashidi, N. A.; Yusup, S., An overview of activated carbons utilization for the post-combustion carbon dioxide capture. *Journal of CO2 Utilization* **2016,** 13, 1-16.
41. Sevilla, M.; Valle-Vigón, P.; Fuertes, A. B., N-Doped Polypyrrole-Based Porous Carbons for CO2 Capture. *Advanced Functional Materials* **2011,** 21, (14), 2781-2787.
42. Shafeeyan, M. S.; Daud, W. M. A. W.; Houshmand, A.; Arami-Niya, A., Ammonia modification of activated carbon to enhance carbon dioxide adsorption: Effect of pre-oxidation. *Applied Surface Science* **2011,** 257, (9), 3936-3942.
43. García, S.; Pis, J. J.; Rubiera, F.; Pevida, C., Predicting Mixed-Gas Adsorption Equilibria on Activated Carbon for Precombustion CO2 Capture. *Langmuir* **2013,** 29, (20), 6042-6052.
44. Dreisbach, F.; Staudt, R.; Keller, J. U., High Pressure Adsorption Data of Methane, Nitrogen, Carbon Dioxide and their Binary and Ternary Mixtures on Activated Carbon. *Adsorption* **1999,** 5, (3), 215-227.
45. Rufford, T. E.; Watson, G. C. Y.; Saleman, T. L.; Hofman, P. S.; Jensen, N. K.; May, E. F., Adsorption Equilibria and Kinetics of Methane + Nitrogen Mixtures on the Activated Carbon Norit RB3. *Industrial & Engineering Chemistry Research* **2013,** 52, (39), 14270-14281.
46. Narasimman, R.; Vijayan, S.; Prabhakaran, K., Carbon foam with microporous cell wall and strut for CO2 capture. *RSC Advances* **2014,** 4, (2), 578-582.
47. Dassanayake, R. S.; Gunathilake, C.; Jackson, T.; Jaroniec, M.; Abidi, N., Preparation and adsorption properties of aerocellulose-derived activated carbon monoliths. *Cellulose* **2016,** 23, (2), 1363-1374.
48. Ribeiro, R. P.; Sauer, T. P.; Lopes, F. V.; Moreira, R. F.; Grande, C. A.; Rodrigues, A. r. E., Adsorption of CO2, CH4, and N2 in Activated Carbon Honeycomb Monolith. *Journal of Chemical & Engineering Data* **2008,** 53, (10), 2311-2317.
49. Toth, J., State Equations of the Solid-Gas Interface Layers. *Acta Chim. Acad. Sci. Hung.* **1971,** 69, 311-328.

50. Myers, A. L.; Prausnitz, J. M., Thermodynamics of mixed-gas adsorption. *AIChE Journal* **1965,** 11, 121-127.
51. Valenzuela, D. P.; Myers, A. L., *Adsorption equilibrium data handbook*. Prentice Hall: Engleword Cliffs, NJ, 1989; p 364.
52. Wu, X.; Niknam Shahrak, M.; Yuan, B.; Deng, S., Synthesis and characterization of zeolitic imidazolate framework ZIF-7 for CO2 and CH4 separation. *Microporous and Mesoporous Materials* **2014,** 190, 189-196.
53. Ribeiro, R. P.; Sauer, T. P.; Lopes, F. V.; Moreira, R. F.; Grande, C. A.; Rodrigues, A. E., Adsorption of CO2, CH4, and N2 in activated carbon honeycomb monolith. *Journal of Chemical & Engineering Data* **2008,** 53, (10), 2311-2317.
54. Cavenati, S.; Grande, C. A.; Rodrigues, A. E., Adsorption Equilibrium of Methane, Carbon Dioxide, and Nitrogen on Zeolite 13X at High Pressures. *Journal of Chemical & Engineering Data* **2004,** 49, (4), 1095-1101.
55. Saha, D.; Bao, Z.; Jia, F.; Deng, S., Adsorption of CO(2), CH(4), N(2)O, and N(2) on MOF-5, MOF-177, and zeolite 5A. *Environ Sci Technol* **2010,** 44, (5), 1820-6.
56. Bao, Z.; Yu, L.; Ren, Q.; Lu, X.; Deng, S., Adsorption of CO2 and CH4 on a magnesium-based metal organic framework. *Journal of Colloid and Interface Science* **2011,** 353, (2), 549-556.

Figure captions

Figure 1 Process block flow diagram of (a) zinc complex templated furfural + 2-aminophenol procedures to produce activated carbons and (b) pyrolysis to char, and then physical activation with CO_2.

Figure 2 SEM images of dry peel from Cavendish bananas (BP).

Figure 3 Thermal gravimetric analysis of dried banana peel (BP) and banana peel-zinc composite impregnated with furfural and 2-aminophenol (BPC) in 20 mL/min N2, heating rate 10 K/min. Weight % is on a dry basis after removal of adsorbed moisture and any other light gases at temperature below to 473 K.

Figure 4 SEM images of soft templated carbon foams (a-c) BPC- 1273-Ar-3h, prepared at 1273 K under argon for 3 hours and (d-f) BPC- 1273-CO_2-1h, prepared at 1273 K under CO_2 for 1 h, and (g-i) example of a CO_2 activated banana peel carbon ACBP-1023-CO_2-1h.

Figure 5 Differential pore volumes versus pore diameter obtained from mercury intrusion porosimetry for BPC-1273-Ar-3h and BPC-1273-CO_2-1h.

Figure 6 XPS survey and high-resoltuion N 1s peak for (a,b) banana peel composite with furfural + 2-aminophenol resin (BPC), (c,d) CBF-1273-Ar-3h and (e,f) CBF-1273-CO_2-1h.

Figure 7 (a) N_2 adsorption-desorption isotherm measured at 77 K on CO_2 activated banana peel carbon BPAC-1023-CO_2-1 and the zinc-complex furfural + 2-aminophenol derived banana peel carbons (CBFs). (b) Pore size distribution determined from isotherms measured at 77 K with N_2.

Figure 8 (a) CO_2 adsorption capacities at 273 K and pressures up to 130 kPa measured with the Micromeritics Tristar II on chemically modified banana peel foams (CBFs) and BPAC-1023-CO_2-1 from direct CO_2 activation of banana peel. (b) Pore size distribution determined from isotherms measured at 273 K with CO_2**.**

Figure 9 CO_2 adsorption capacities at 303 K for chemically-modified banana foams and activated carbons measured at pressures up to 130 kPa on the Micromeritics Tristar II.

Figure 10 Relationship between the CO_2 uptake capacity and (a) nitrogen content and (b) micropore surface area.

Figure 11 Measured and modelled CO_2 adsorption capacities for soft templated carbon foam CBF-1273-CO_2-1h at temperatures of 298 K, 313 K and 323 K. (a) Absolute adsorption capacities. The lines represent the predictions of the Toth model (Eq. 4). (b) Deviations between the measured and the calculated adsorption capacities.

Figure 12 Measured and modelled CH_4 adsorption capacities for soft templated carbon foam CBF-1273-CO_2-1h at temperatures of 298 K, 313 K and 323 K. (a) Absolute adsorption capacities. The lines represent the predictions of the Toth model (Eq. 4). (b) Deviations between the measured and the calculated adsorption capacities.

Figure 13 Measured and modelled N_2 adsorption capacities for soft templated carbon foam CBF-1273-CO_2-1h at temperatures of 298 K, 313 K and 323 K. (a) Absolute adsorption capacities. The lines represent the predictions of the Toth model (Eq. 4). (b) Deviations between the measured and the calculated adsorption capacities.

Figure 14 CO_2, CH_4 and N_2 absolute adsorption capacities at 298 K on CBF-1273-Ar-3h measured on the Belsorb-BG.

Figure 15 Selectivity of CBF-1273-CO_2-1h predicted by IAST from equimolar mixtures of CO_2 + N_2, CO_2 + CH_4 and CH_4 + N_2 as a function of pressure at 298 K.

Table 1 Carbon product yield, proximate analysis by ASTM D 7582-10 using TGA and elemental composition measured by CHNS/O analyser.

Sample	Description of carbon form	Yield (%)	ASTM D 7582-10			Elemental Composition (%)		
			Fixed carbon (%wt)	Volatiles (%wt.)	Ash (%wt)	N	C	H
BP-Raw	-	-	24.2	67.7	8.2	1.9	42.0	5.6
BP-char	Agglomerated carbon particles	38.8	65.8	21.6	12.7	2.1	48.8	1.1
BPC	-	-	40.8	45.9	13.3	8.0	32.4	3.6
CBF-1023-Ar-3h	Monolith carbon	65.7	66.1	22.3	11.6	6.0	47.5	0.7
CBF-1273-Ar-3h	Monolith carbon	30.1	84.7	10.7	4.6	4.6	70.0	1.3
CBF-1273-Ar-8h	Monolith carbon	26.4	82.3	12.2	5.4	4.5	70.4	1.2
CBF-1273-Ar-11h	Monolith carbon	23.6	85.6	10.5	3.9	3.9	70.4	1.0
CBF-1023-CO_2-3h	Monolith carbon	45.2	55.8	32.3	11.9	3.9	27.4	1.1
CBF-1123-CO_2-3h	Monolith carbon	24.6	44.4	31.9	23.7	4.0	30.2	1.4
CBF-1273-CO_2-1h	Monolith carbon	14.2	76.3	16.2	7.5	4.2	43.5	2.2
BPAC-1023-CO_2-1h	Agglomerated carbon particles	67.9	60.1	28.6	11.3	2.3	33.8	1.5

Table 2 Surface textural properties of zinc complex templated carbon foams from banana peel (CBFs) and a CO_2 activated banana peel carbon (BPAC-1023-CO_2-1h) determined from sorption isotherms of N_2 at 77 K and CO_2 at 273 K.

Sample	N_2				CO_2	
	D-A Micropore Surface area ($m^2 \cdot g^{-1}$)	Micropore Volume ($cm^3 \cdot g^{-1}$)	BET surface area ($m^2 \cdot g^{-1}$)	Pore volume ($cm^3 \cdot g^{-1}$)	D-R Micropore Surface area ($m^2 \cdot g^{-1}$)	Micropore Volume ($cm^3 \cdot g^{-1}$)
CBF-1023-Ar-3h	102.7	0.04	91.5	0.093	337	0.14
CBF-1273-Ar-3h	198.3	0.07	169	0.18	620.9	0.29
CBF-1273-Ar-8h	225.7	0.08	183.6	0.19	675.5	0.31
CBF-1273-Ar-11h	228.7	0.08	190.4	0.17	628.5	0.3
CBF-1023-CO_2-3h	446.7	0.16	352.2	0.22	369.3	0.23
CBF-1123-CO_2-3h	644.7	0.26	533.6	0.31	365.3	0.35
CBF-1273-CO_2-1h	1611	0.56	1426.1	0.83	881.93	1.09
BPAC-1023-CO_2-1h	234.1	0.11	204.3	0.11	299.9	0.27

Table 3 Surface nitrogen concentrations and functional groups on the intermediate banana peel + fufural + 2-aminophenol composite (BPC) and chemically modified banana peel carbon foam (CBFs) surfaces determined using XPS; N-1: primary amine groups, N-2: amide groups, N-3: nitrates, N-4: pyridine, N-5: pyrrol or other forms of pyridine like nitrogens, N-6: quaternary nitrogen.

Sample	Overall N content (%)	Overall O content (%)	N–1 (%)	N–2 (%)	N–3 (%)	N–4 (%)	N–5 (%)	N–6 (%)
			399.4 ± 0.1 eV	400.5 ± 0.1 eV	407.3 ± 0.1 eV	398.2 ± 0.1 eV	399.8 ± 0.1 eV	401.1 ± 0.1 eV
			Schematic					
			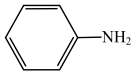	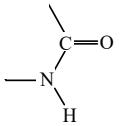	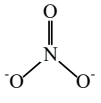		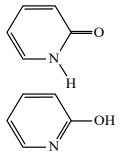	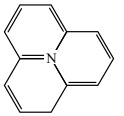
BPC	20.6	6.9	36.9	21.6	41.5	-	-	-
CBF-1273-Ar-3h	7.5	4.6	-	-	-	37.8	17.9	44.3
CBF-1273-CO_2-1h	10	4.9	-	-	-	38.7	37.2	24.1

Table 4 Fitting parameters of the Toth Model for CO_2, CH_4 and N_2 on CBF-1273-CO_2-1h

Gas	Toth model				
	$Q_{max,i}$ (mmol·g^{-1})	$b_{0,i}.10^6$ (MPa)	$-\Delta H_{Toth,i}$ (J·mmol^{-1})	t_i	SD (mmol·g^{-1})
CO_2	15.77	0.625	24.0	0.4	0.083
CH_4	8.19	0.655	20.4	0.56	0.035
N_2	5.75	1.25	15.7	0.71	0.009

Table 5 Equilibrium capacity of adsorbents in literature and ACD for CO_2, CH_4 and N_2 at 100 kPa and 1000 kPa at measurement pressure close to 298 K.

Adsorbent	CO_2 capacity (mol/kg)		CH_4 capacity (mol/kg)		N_2 capacity (mol/kg)	
	100 kPa	1000 kPa	100 kPa	1000 kPa	100 kPa	1000 kPa
Banana peel derived carbon CBF-1273-CO2-1h (this work)	2.70	6.83	1.00	3.51	0.35	1.79
Monolith from tar pitch and coal powder. KOH activated.[19]	3.2	6.54	1.46	3.96	0.54	2.27
Activated carbon honeycomb monolith [53]	3.0	-	1.4	-	0.5	-
Norit RB1 extra activated carbon [44]	2.20	7.60	1.22	2.89	0.39	2.02
Zeolite13X [54]	3.3	6.40	0.59	2.90	0.28	1.83
Metal organic framework MOF-177 [55]	1.59	-	0.63	-	0.17	-
Metal organic framework Mg-MOF-74[56]	8.5	-	1.0	-	-	-

Supporting Information captions

Fig. S1 SEM images of (a-c) the dry banana peel precursor (BP) and (d-f) banana peel derived char (BP-char) pyrolysed at 873 K for 1 hour.

Fig. S2 EDX analysis of (a) BPC- (b) BPC-1023-Ar-3h (c) BPC-1273-Ar-3h**.**

Fig. S3 Predicted IAST selectivity of CO_2/CH_4, CO_2/N_2 and CH_4/N_2 at 298 K based on the Toth model regression data as a function of mixture composition.

Table S 1 Measured absolute adsorption capacities for CO_2, CH_4, and N_2 on BPC-1273-CO_2-1h at 298 K, 313 K and 323 K, and the corresponding uncertainty $u(Q_{abs})$.

Table S 2 Measured absolute adsorption capacities for CO_2, CH_4,and N_2 on BPC-1273-Ar-3h at 298 K measured with the Belsorb-BG.

SUPPORTING INFORMATION

Nitrogen-Doped Carbon Foams Synthesized from Banana Peel and Zinc Complex Template for Adsorption of CO_2, CH_4, and N_2

Arash Arami-Niya, Thomas E. Rufford* and Zhonghua Zhu

School of Chemical Engineering, The University of Queensland, St Lucia 4072 Australia

Description of high pressure gravimetric adsorption apparatus

Adsorption isotherms of pure fluids CH_4, CO_2 and N_2 on the CBF carbons were measured at (298, 313 and 323) K and pressures up to 4000 kPa using a BELSORP-BG instrument (BEL Japan) equipped with a RUBOTHERM magnetic floating balance. Prior to adsorption measurements the carbon foam was degassed in-situ at 473 K for 24 hrs.

The balance records three different positions during a single step of an adsorption measurement: (1) a *zero point* (ZP) is used to correct any drift in the balance between data points in an isotherm measurement; (2) *measuring point 1* (m_{bal}) records the location of the balance during the measurement and indicates the total weight change; and (3) after the system reaches adsorption equilibrium *measuring point 2* records the balance position when a titanium sinker of about 4.5 cm^3 volume is lifted. *Measuring point 2* is used to determine the fluid density, ρ_f, at the equilibrium pressure and temperature conditions.

The absolute mass of adsorbed gas (m_a) is determined from the weight recorded at measuring point 1 (m_{bal}) by a force balance on the system as shown in Equation 3:

$$m_{bal} = m_b + m_s + m_a - (V_b + V_s + V_a)\rho_f \quad (3)$$

The force balance includes the mass of the sample basket and balance hook (m_b), the mass of the solid adsorbent (m_s), and application of Archimedes principle to correct for the buoyancy effect of the fluid on the volume $(V_b + V_s + V_a)$. Here, V_b is the volume of basket and hook, V_s is the volume of the solid adsorbent not accessible to the adsorbate, and V_a the volume of the adsorbed phase. At our measurement conditions the volume of the adsorbed phase is negligible compared to $V_b + V_s$ and may be ignored from the buoyancy correction term. The empty basket volume V_b is obtained from a calibration measurement made with helium across the range of temperatures and pressures of interest for the adsorption measurements. The masses of the degassed basket and sample are measured under an ultimate vacuum of 1×10^{-5} Torr, a condition at which the buoyancy effect can be considered negligible since ρ_f is essentially zero. The weight measurement resolution and reproducibility of the mass balance are 10^{-5} g and $\pm3\times10^{-5}$ g (STD) and the density resolution and accuracy of the unit are 2×10^{-6} and $\pm2\times10^{-5}$ g·cm^{-3}, respectively.

Absolute equilibrium adsorption capacity in mmol.g^{-1} ($Q_{abs,i}$) of species *i* with molecular weight MW_i was calculated from the m_a measured on the BELSORP-BG by:

$$Q_{abs,i} = MW_i\left(\frac{m_a}{m_s}\right) \quad (4)$$

Fig. S1 SEM images of (a-c) the dry banana peel precursor (BP) and (d-f) banana peel derived char (BP-char) pyrolysed at 873 K for 1 hour.

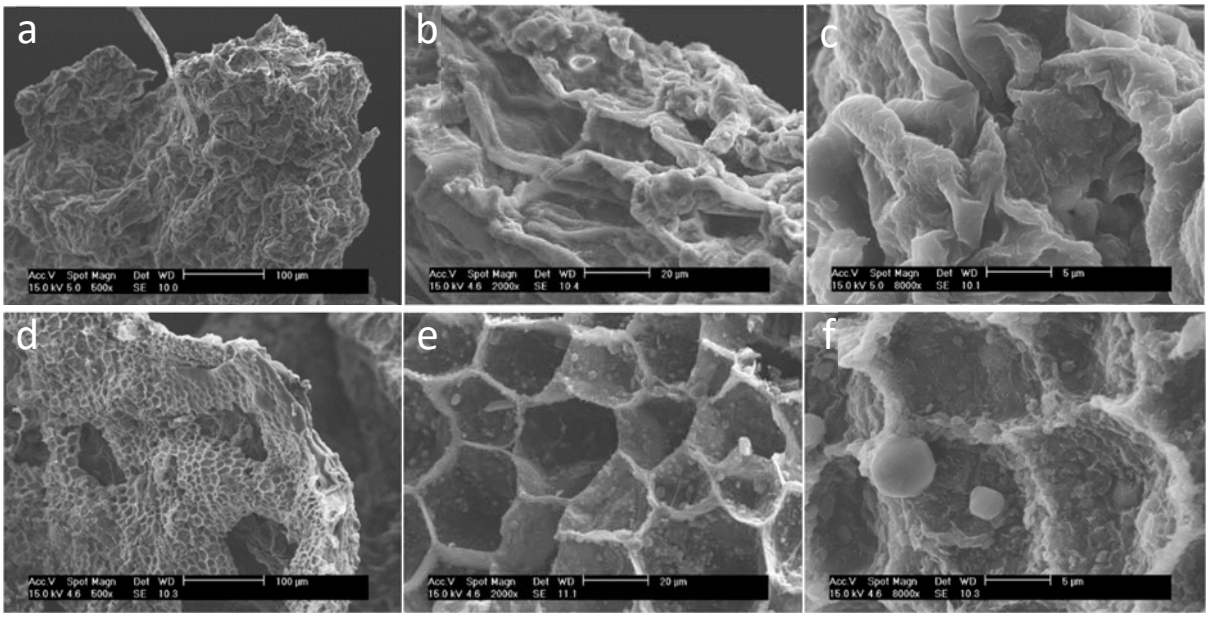

Fig. S2 EDX analysis of (a) BPC- (b) CBF-1023-Ar-3h (c) CBF-1273-Ar-3h**.**

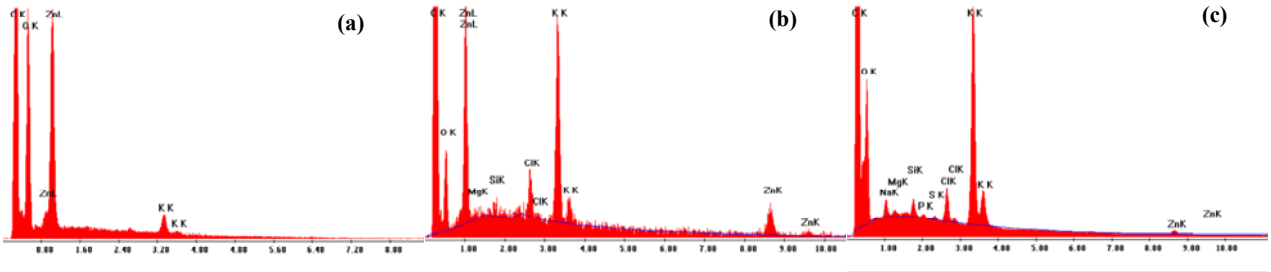

Table S1 Measured absolute adsorption capacities for CO_2, CH_4, and N_2 on CBF-1273-CO_2-1h at 298 K, 313 K and 323 K, and the corresponding uncertainty $u(Q_{abs})$.

T=298 K		T=313 K		T=323 K	
P (kPa)	$Q_{abs,\,i}$ (mmol·g^{-1})	P (kPa)	$Q_{abs,\,i}$ (mmol·g^{-1})	P (kPa)	$Q_{abs,\,i}$ (mmol·g^{-1})
			CH_4		
29.89	0.43	29.18	0.30	28.71	0.24
59.89	0.70	61.31	0.55	61.64	0.45
100.11	1.00	101.71	0.78	102.38	0.67
202.30	1.57	201.78	1.25	202.81	1.09
401.25	2.30	401.20	1.90	402.26	1.68
700.65	3.02	700.93	2.55	701.57	2.30
999.81	3.51	1000.59	3.00	1000.71	2.72
1498.23	4.07	1499.01	3.54	1498.92	3.24
1997.03	4.47	1998.63	3.90	1998.70	3.62
2496.30	4.75	2497.30	4.18	2497.15	3.89
2996.03	4.98	2996.42	4.39	2996.05	4.11
3494.84	5.15	3494.63	4.56	3494.96	4.29
3991.82	5.29	3994.20	4.68	3994.78	4.42
			CO_2		
29.07	1.45	27.67	1.07	29.47	0.88
59.03	2.09	59.29	1.62	59.48	1.34
99.20	2.70	99.58	2.13	99.63	1.78
198.77	3.73	199.06	3.02	199.61	2.58
398.51	4.98	398.59	4.16	398.95	3.61
698.04	6.10	698.50	5.22	698.76	4.60
997.88	6.83	998.53	5.93	998.26	5.28
1497.15	7.64	1497.54	6.75	1497.71	6.06
1996.68	8.19	1996.14	7.31	1996.72	6.60
2495.35	8.58	2496.84	7.71	2495.54	7.00
2994.02	8.86	2994.79	8.01	2996.20	7.31
3494.05	9.06	3495.03	8.24	3495.48	7.54
3995.92	9.21	3997.10	8.42	3996.14	7.73
			N_2		
27.21	0.10	27.11	0.08	25.75	0.08
60.46	0.22	60.51	0.16	60.15	0.15
100.98	0.35	100.93	0.26	100.22	0.21
200.99	0.62	201.83	0.47	202.24	0.41
401.70	1.02	401.78	0.81	401.94	0.71
700.29	1.47	701.14	1.20	701.17	1.07
999.86	1.79	1000.14	1.50	1000.82	1.35
1498.19	2.22	1498.71	1.91	1498.95	1.71
1997.84	2.55	1997.62	2.22	1998.28	2.01
2496.12	2.80	2497.08	2.45	2497.31	2.24
2996.23	3.00	2996.09	2.67	2997.26	2.45
3494.97	3.15	3496.47	2.84	3495.83	2.61
3994.17	3.29	3994.11	2.98	3994.41	2.75

Table S2 Measured absolute adsorption capacities for CO_2, CH_4,and N_2 on CBF-1273-Ar-3h at 298 K measured with the Belsorb-BG.

T (K)	P (kPa)	$Q_{abs,i}$ (mmol·g^{-1})	$u\left(Q_{ex,i}\right)$ (mmol·g^{-1})
		CO_2	
298.1	22.9	1.559	2.70203E-07
298.2	58.0	2.251	9.96551E-05
298.2	100.0	2.695	0.000229584
298.2	199.2	3.350	0.000109809
298.1	398.3	3.995	0.000150915
298.2	698.4	4.457	1.34571E-05
298.1	998.4	4.759	0.001588641
298.1	1496.8	5.042	0.000734312
298.1	1995.0	5.237	0.0006978
298.1	2493.6	5.388	0.003072683
298.1	2992.2	5.483	0.002238461
298.1	3491.3	5.558	0.003037111
		CH_4	
298.1	27.7	0.151	0.001003
298.1	59.7	0.296	0.001885
298.1	100.3	0.682	0.00221
298.1	199.2	0.933	0.007507
298.1	398.2	1.355	0.013127
298.1	698.4	1.733	0.022505
298.2	994.9	1.990	0.034388
298.1	1497.2	2.313	0.050049
298.1	1996.7	2.581	0.066126
298.1	2496.0	2.740	0.085154
298.1	2994.7	2.845	0.096217
298.1	3494.9	2.971	0.111876
298.1	3994.1	3.069	0.133368
		N_2	
298.3	28.2	0.135	0.001206
298.3	60.0	0.248	0.003252
298.3	100.4	0.366	0.005468
298.3	200.1	0.699	0.010502
298.3	400.3	1.008	0.018697
298.3	699.7	1.374	0.030467
298.3	999.7	1.600	0.040895
298.2	1498.6	1.874	0.057201
298.2	1998.1	2.092	0.04947
298.2	2496.6	2.234	0.054754
298.2	2995.9	2.327	0.059223
298.2	3496.2	2.420	0.064235
298.2	3995.1	2.472	0.069111

Equilibrium selectivity

Beside the absolute capacity of a potential adsorbent, the selectivity for one component from the other species is an important parameter in gas separation processes. To evaluate the gas separation potential of BPC-1273-CO_2-1h, we calculated the adsorption equilibrium selectivity for separating CO_2 + CH_4, CO_2 + N_2 and CH_4 + N_2 gas mixture pairs using the ideal adsorbed solution theory (IAST). The selectivity of the mentioned gas mixtures calculated at 298 K based on pure-component adsorption isotherms using the fitted Toth equilibrium model. The predicted IAST selectivity at 298 K and 100 kPa for different gas mixture compositions were presented in Fig. S3(a-c).

The ideal equilibrium selectivity, α_{ij}, can be defined as:

$$\alpha_{ij} = \left(\frac{x_i}{x_j}\right)\left(\frac{y_j}{y_i}\right)_{if(y_i=y_j)} \rightarrow \alpha_{ij} = \left(\frac{Q_{\mu i}}{Q_{\mu j}}\right) \quad (3)$$

where y and x are the mole fraction of component *i* and *j* in the vapour and adsorbed phases, respectively.

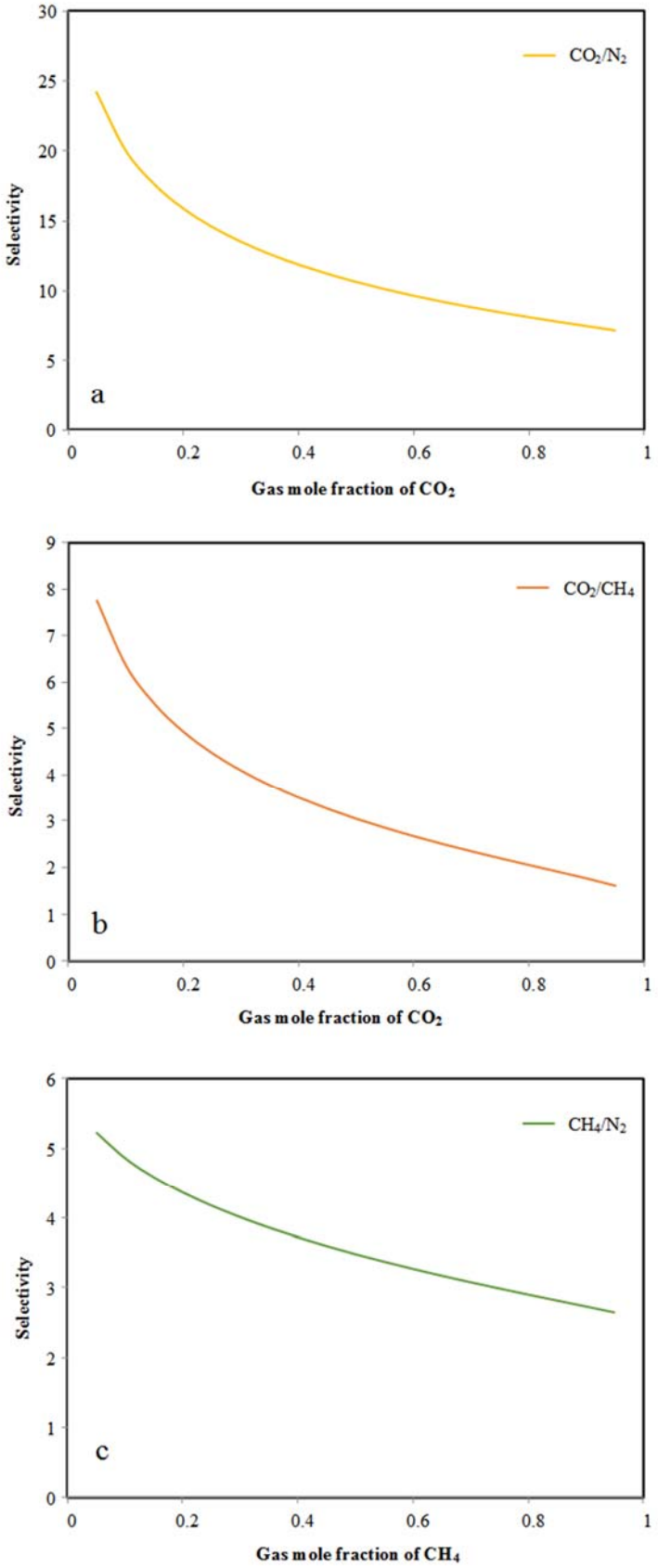

Fig. S3 Predicted IAST selectivity of CO_2/N_2, CO_2/CH_4, and CH_4/N_2 at 298 K based on the Toth model regression data as a function of mixture composition.